Magnetocaloric effect in {Cu₃}-type compounds using the Heisenberg antiferromagnetic model in a triangular ring

G. A. Antonio,[1] J. Torrico [●],[2] A. S. da Mata [●],[1] S. M. de Souza,[1] and O. Rojas [●][1]

[1]*Department of Physics, Institute of Natural Science, Federal University of Lavras, 37200-900 Lavras, Minas Gerais, Brazil*
[2]*Departamento de Física, Instituto de Ciências Exatas, Universidade Federal de Alfenas, 37133-840 Alfenas, Minas Gerais, Brazil*

In this work we present a theoretical investigation into an antiferromagnetically coupled spin system, specifically, Cu₃-*X* (*X*=As, Sb), which exhibits an isosceles triangular configuration or slightly distorted equilateral triangular configuration, as previously identified by Choi *et al.* [Phys. Rev. Lett. **96**, 107202 (2006)]. This system can be effectively represented by the Heisenberg model on a triangular structure, taking into account the exchange interaction, the Dzyaloshinskii-Moriya interaction, *g* factors, and external magnetic field, as delineated in the previous work. By using a numerical approach we explore both zero-temperature and finite-temperature behaviors of a Cu₃-type antiferromagnetically coupled spin system. At zero temperature, the system displays a 1/3 quasiplateau magnetization when the magnetic field is varied. Moreover, we place particular emphasis on the magnetic properties, including magnetization, magnetic susceptibility, entropy, and specific heat at finite temperatures. Furthermore, we investigate the magnetocaloric effect as a function of an externally imposed magnetic field, oriented both parallel and perpendicular to the plane of the triangular structure. Interestingly, these configurations demonstrate remarkably similar behavior for both orientations of the magnetic field. Our investigation also includes an analysis of the adiabatic curve, the Grüneisen parameter, and the variation in entropy when magnetic field is applied or removed. The magnetocaloric effect is found to be more prominent in low the temperature region, typically at $T \sim 1$ K, for both parallel and perpendicular magnetic fields at ∼4.5 and ∼5 T, respectively.

I. INTRODUCTION

The study of spin systems with antiferromagnetic coupling has drawn significant attention in the field of condensed matter physics. These systems exhibit interesting features that arise from the interplay of various factors that can be investigated through their magnetic properties. Moreover, understanding the characteristics of these systems helps to clarify their potential applications in areas such as magnetocaloric materials and spintronics.

The magnetocaloric effect (MCE) is a phenomenon that has been studied extensively due to its potential applications in magnetic refrigeration and cooling technologies. Initially observed in the late 19th century, it refers to the change in temperature that occurs when a magnetic material is subjected to a varying magnetic field, a phenomenon resulting from the intrinsic magnetic properties of the material [1,2]. The reversibility of this effect was confirmed in later studies, sparking significant interest [2]. The MCE has been observed in a variety of materials, such as rare earth alloys, magnetic oxides, and transition metals, with notable instances of a giant magnetocaloric effect (GMCE) driven by structural transitions [3,4]. In 1951, Darby and colleagues made a pioneering step in the field by designing a two-stage magnetocaloric regenerator using materials with different Curie points, achieving temperature down to final values as low as 3 mK at an induction of 0.42 T [5].

The concept of magnetic refrigeration at room temperature was introduced almost a century after the discovery of MCE. In 1976, Brown developed an efficient refrigeration system using gadolinium, marking a significant advancement [6]. Following this, in the late 1990s, Pecharsky and Gschneidner discovered GMCE at room temperature in gadolinium germanium silicon alloys (Ga-Ge-Si) [7]. Around the same time, Zimm proposed a prototype showcasing the feasibility of magnetic refrigeration near room temperature [8]. These developments led to substantial experimental and theoretical research on bulk (Mn, Fe)₂(P, Si)-based GMCE materials [7,9–12].

Nanoscale materials with GMCE have gained attention due to their high surface-to-volume ratio, enhanced interactions, and rapid thermal response. These characteristics make them valuable for temperature control applications. Examples of such applications include a room-temperature thermal diode [13], a self-pumping magnetic cooling device using Mn-Zn ferrite nanoparticles that achieves efficient energy conservation without external energy input [14], a magnetic cooling device based on a ferrofluid thermomagnetic that can effectively transfer heat over large distances [15], control of ferrofluid droplets in microfluidics [16], and a magnetostructural phase transition in Ni-Mn-Ga films showing a strong MCE at low magnetic fields [17]. Other applications involve thick gadolinium films for energy conversion mechanisms [10,11] and biomedical applications like magnetic hyperthermia [18] and efficient drug delivery via nanocarriers [19].

Furthermore, the study of magnetic materials has attracted significant attention due to their wide range of potential technological applications in fields such as spintronics,

nanoscale engineering, and biomedicine. This has prompted investigations of $S = 1/2$ antiferromagnetic triangular spin rings, which might be ideal for observing peculiar quantum magnetization due to two doublets. The compounds investigated include spin-frustrated $(VO)_3^{6+}$-triangle-sandwiching octadecatungstates as molecular magnets, displaying unusual magnetization jumps due to predicted half-step or 1/3-plateau magnetization [20]. Experiments on a Cu$_3$ nanomagnet revealed half-step magnetization, hysteresis loops, and an asymmetric magnetization between negative and positive fields in a fast-sweeping external field, which can be ascribed to an adiabatic change in magnetization [21]. Reference [22] investigated the spin-electric coupling. The $S = 1/2$ spin triangle clusters were also investigated, revealing that the magnetization behavior and spin configurations are significantly affected by the diamagnetic heteroatom ($X =$ As and Sb) [23]. These clusters show potential for implementing spin-based quantum gates [24]. Bouammali *et al.* [25] explored the antisymmetric exchange in a tri-copper II complex, highlighting its origins, theoretical implications, and potential for more advanced electronic structure calculations. A spin-frustrated trinuclear copper complex based on triaminoguanidine demonstrates strong antiferromagnetic interactions with negligible antisymmetric exchange [26]. Several other studies have also examined triangular copper structures [27–31].

On the other hand, theoretical investigations to explore various properties of nanomagnets or magnetic molecular clusters, beyond experimental results, are highly significant. For instance, Kowalewska and Szałowski conducted a theoretical study of the magnetocaloric properties of V$_6$, a polyoxovanadate molecular magnet. Their research, using numerical diagonalization and field ensemble formalism, uncovered highly tunable magnetocaloric effects [32]. Karľová *et al.* studied the magnetization in antiferromagnetic spin-1/2 XXZ Heisenberg clusters, demonstrating additional magnetization plateaus due to quantum interaction and an enhanced magnetocaloric effect near magnetization shifts [33]. Reference [34] employed exact diagonalization to examine the spin-1/2 Hamiltonian for coupled isosceles Heisenberg triangles, yielding a zero-temperature quantum phase transition diagram and a magnetization profile. The authors also analyzed the thermodynamic behavior and MCE. Another theoretical study was conducted on a Cu$_5$ pentameric molecule using a spin-1/2 Heisenberg model, which explored the thermodynamic properties, phase diagram, magnetization, and magnetocaloric effects [35]. A theoretical study of the MCE in paramagnetic PrNi$_2$ revealed an unexpected inverse effect due to an anomalous increase in magnetic entropy at low temperatures [36]. Several other theoretical investigations can be found in references therein [32–36].

In this context, a system of interest is Cu$_3$-X (X=As, Sb), which adopts an isosceles triangular or slightly distorted equilateral triangular configuration. Previously, Choi *et al.* [21,23,24] established that the behavior of this system can be effectively described by the Heisenberg model on a triangular structure, incorporating elements such as exchange interaction, Dzyaloshinskii-Moriya interaction, g factors, and external magnetic fields. Exploring the magnetic properties

and thermodynamic behavior of this Cu$_3$-type spin system is important because it helps us understand its fundamental characteristics and identify potential advantages for its applications.

This paper is organized as follows: in Sec. II we present the model and analyze some fundamental properties. In Sec. III we explore the main thermodynamic properties. In Sec. IV we discuss the magnetocaloric effect. Finally, in Sec. V we give our conclusions.

II. MODEL

In this work, we aim to explore the thermodynamics and magnetic properties of the triangular cluster Na$_9$[Cu$_3$Na$_3$(H$_2$O)$_9$(α-XW$_9$O$_{33}$)$_2$] (where X=As and Sb), hereinafter referred to as the {Cu$_3$-X} system [21]. The compound under consideration contains three copper atoms, each of which loses two electrons to form a Cu II or Cu^{+2} ion. The electron loss in Cu II ions occurs from both the $4s$ and one of the $3d$ orbitals, resulting in a single unpaired electron and a net magnetic moment with a spin of $S = 1/2$; this behavior can be adequately described by the Heisenberg model within the framework of an isosceles triangular spin ring [21,23,24]. Consequently, we adopt the Hamiltonian presented in previous works [21,23,24] that characterizes Cu$_3$-type compounds as follows:

$$\mathbf{H} = \sum_{j=1}^{3} \sum_{\alpha=x,y,z} J_{j,j+1}^{\alpha} S_j^{\alpha} S_{j+1}^{\alpha}$$
$$+ \sum_{j=1}^{3} [\mathbf{D}_{j,j+1} \cdot (\mathbf{S}_j \times \mathbf{S}_{j+1}) + \mu_B \mathbf{S}_j \cdot \mathbf{g}_j \cdot \mathbf{B}_j], \quad (1)$$

where S_j^{α} denotes the spin-1/2 components of localized Cu$_3$-type spin with $\alpha = \{x, y, z\}$ and $J_{j,j+1}^{\alpha}$ (simplified to J_j^{α}) represents the exchange interaction parameters between sites j and $j + 1$ for each component (for a schematic view see Refs. [21,23,24]). The second term refers to the Dzyaloshinskii-Moriya interaction vector $\mathbf{D}_{j,j+1}$, denoted as $\mathbf{D}_{j,j+1} = (D_{j,j+1}^x, D_{j,j+1}^y, D_{j,j+1}^z)$. The site-dependent g factors are defined as $\mathbf{g}_j = (g_j^x, g_j^y, g_j^z)$, while the last term corresponds to the magnetic field $\mathbf{B}$, which we assume is independent of the spin site on the triangle. Here, μ_B denotes the Bohr magneton. The specific parameters were obtained using electron spin resonance data [21,23,24], and these parameters are reproduced in Table I for both compounds. It is worth mentioning that only $\mathbf{D}_{1,2} = (D, D, D)$ is isotropic, while $\mathbf{D}_{2,3}$ and $\mathbf{D}_{3,1}$ contribute solely to the z component, expressed as $\mathbf{D}_{2,3} = \mathbf{D}_{3,1} = (0, 0, D)$. Other interactions, such as the crystal field effect and magnetocrystalline anisotropy, were disregarded in this study because their contributions are not deemed highly relevant, as supported by Refs. [21,31].

For convenience, we express the Hamiltonian (1) in kelvins. Hence, let us redefine μ_B as $\hat{\mu}_B = \frac{\mu_B}{k_B} = 0.6717156644$ K/T, where k_B denotes the Boltzmann constant. Therefore, the magnetic field $\mathbf{B}$ is conveniently measured in teslas. This is equivalent to setting the Boltzmann constant as $k_B = 1$, implying that, for the sake of simplicity, all calculations will be expressed in units of k_B.

TABLE I. Magnetic parameters of the $\{Cu_3\text{-}X\}$ compounds, where X denotes either As or Sb, as extracted from Ref. [23].

Magnetic parameters	Notation	{Cu₃-As}	{Cu₃-Sb}
$J_{1,2}^x = J_{1,2}^y$	J_1	4.50 K	4.49 K
$J_{1,2}^z$	J_1^z	4.56 K	4.54 K
$J_{2,3}^x = J_{2,3}^y = J_{3,1}^x = J_{3,1}^y$	J_2	4.03 K	3.91 K
$J_{2,3}^z = J_{3,1}^z$	J_2^z	4.06 K	3.96 K
$D_{1,2}^z = D_{2,3}^z = D_{3,1}^z$	D	0.529 K	0.517 K
$D_{1,2}^x = D_{1,2}^y$	D	0.529 K	0.517 K
$g_1^x = g_1^y$	g_1	2.25	2.24
$g_2^x = g_2^y$	g_2	2.10	2.11
$g_3^x = g_3^y$	g_3	2.40	2.40
$g_1^z = g_2^z = g_3^z$	g_z	2.06	2.07

III. THERMODYNAMICS QUANTITIES

The eigenvalues of the above-mentioned Hamiltonian (1) can be obtained by direct numerical diagonalization. More details about the energy spectra can be found in Refs. [21,23,24], so let us assume that the eigenvalues can be expressed as follows:

$$\mathbf{UHU}^{-1} = \mathbf{E} = \mathrm{diag}(\varepsilon_1, \varepsilon_2, \ldots, \varepsilon_8), \qquad (2)$$

where $\mathbf{U}$ is an 8×8 matrix that diagonalizes the Hamiltonian (1). It is important to note that this matrix, which naturally depends on the Hamiltonian parameters, can be obtained only numerically for a fixed magnetic field.

Thus, the partition function can symbolically be represented by

$$\mathcal{Z} = \mathrm{tr}(e^{-\mathbf{E}/T}) = \sum_{i=1}^{8} e^{-\varepsilon_i/T}. \qquad (3)$$

Here, the eigenvalues ε_i (in kelvins) depend on the Hamiltonian parameters provided in Table I, as well as the magnetic field $\mathbf{B}$ (in teslas), while T represents the temperature of the system (in kelvins). In theory, any physical quantity can be derived from the partition function (3). However, as the eigenvalues can be obtained only numerically, physical quantities that require derivatives, such as magnetization and magnetic susceptibility, among others, must be calculated with caution. Numerical derivatives may not always provide accurate results; hence, it is advisable to avoid them as much as possible. Therefore, we will combine numerical and analytical calculations to safely obtain all physical quantities.

In this regard, the free energy can be denoted by the expression

$$f = -T \ln(\mathcal{Z}). \qquad (4)$$

It should be noted that the free energy is also represented in units of k_B.

A. Internal energy

The first quantity we will discuss is the internal energy, as it directly influences the magnitude of the magnetocaloric effect. As previously stated, the eigenvalues of the Hamiltonian can be obtained using the parameters listed in Table I and a fixed magnetic field. Formally, the average internal energy can
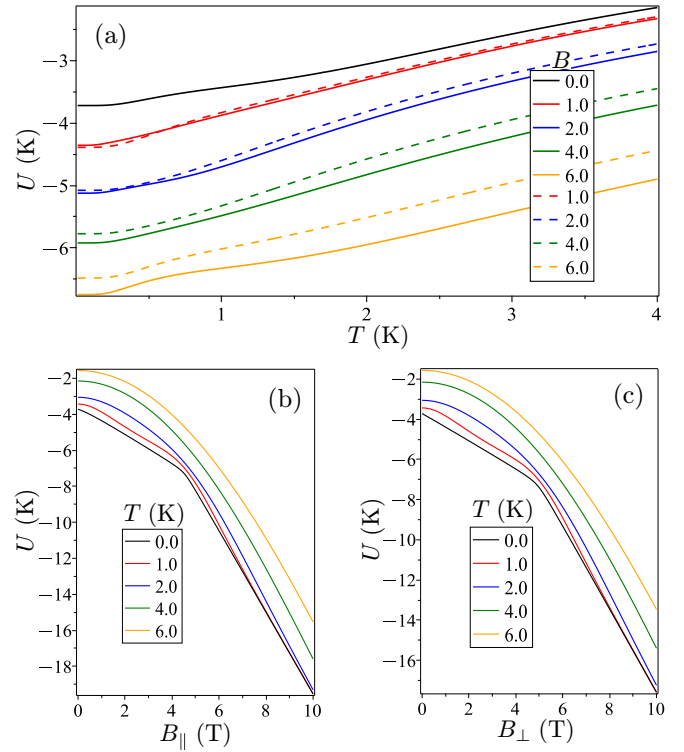

FIG. 1. (a) Internal energy U as a function of temperature; solid lines correspond to $B_\perp$, while dashed lines correspond to $B_\parallel$. (b) and (c) Internal energy U as a function of perpendicular and parallel external magnetic field, respectively. These plots are specifically for the Cu₃-As compound.

be represented as

$$U = \langle \mathbf{H} \rangle = \frac{1}{\mathcal{Z}} \mathrm{tr}\{\mathbf{H} e^{-\mathbf{H}/T}\} = \frac{1}{\mathcal{Z}} \sum_{i=1}^{8} \varepsilon_i e^{-\varepsilon_i/T}. \qquad (5)$$

For the purposes of our discussion, we will focus on the Cu₃-As compound. The Cu₃-Sb compound exhibits analogous characteristics because the parameters given in Table I are quite similar.

Figure 1(a) depicts the internal energy U as a function of temperature, assuming a constant external magnetic field parallel to the triangular plane (solid line) and perpendicular to it (dashed line). The internal energy varies slightly between the parallel and perpendicular magnetic fields. However, as the magnetic field increases, the discrepancy becomes more pronounced. In contrast, Figs. 1(b) and 1(c) show the internal energy as a function of the parallel and perpendicular external magnetic fields, respectively. These plots assume several fixed temperatures, as specified inside the legend. At zero temperature, we observe a significant change in internal energy at $B_\parallel \approx 4.5$ T. Above this magnetic field, the system aligns entirely parallel to the magnetic field, while for $B_\parallel \lesssim 4.5$ T, the configuration comprises two aligned spins and a third with opposite alignment. We observe similar behavior when the external magnetic field acts perpendicularly to the triangular plane, but the shift occurs at a slightly higher magnetic field, $B_\perp \approx 5$ T. This similarity was previously observed in energy spectra and zero-temperature magnetization [21,23,24].
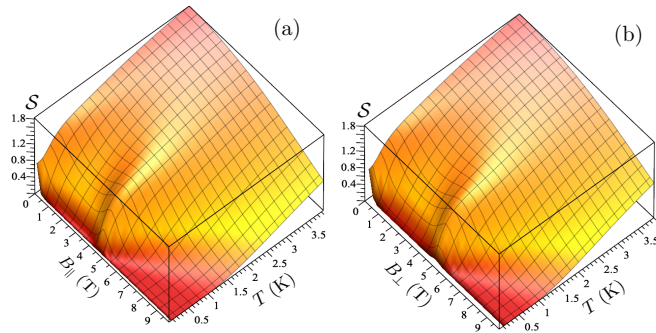
FIG. 2. (a) Entropy $\mathcal{S}$ in the plane of temperature (in kelvins) and parallel external magnetic field (teslas). (b) Entropy $\mathcal{S}$ in the plane of temperature (in kelvins) and perpendicular external magnetic field (teslas). These visualizations are based on the Cu$_3$-As compound.

As temperature increases, this curvature smooths out. In the absence of an external magnetic field, these spin moments are oriented randomly, leading to a higher internal energy state. When an external magnetic field is applied, the spins align with the field, reducing the internal energy of the compound. This variation of energy manifests as a change in the compound temperature, representing the core of the magnetocaloric effect.

B. Entropy

Entropy calculation is relevant because it plays a crucial role in the MCE, essentially serving as the "driving force" to understand both the direct and inverse MCEs, which we will discuss next. As such, entropy is fundamental to understanding the mechanism of the MCE and is pertinent in applications such as magnetic refrigeration. Consequently, entropy can be derived from the internal energy with the following relation:

$$\mathcal{S} = \frac{\langle \mathbf{H} \rangle - f}{T}. \tag{6}$$

In Fig. 2(a) the entropy is illustrated in the plane of temperature (in kelvins) and parallel external magnetic field (teslas). It is worth nothing that $B_{\parallel} \approx 4.5\text{T}$, where the entropy increases very fast in the low-temperature region; this is because the region dominated by two spins aligned with the magnetic field and one spin opposite it changes to a region with all spins aligned with the magnetic field. Similarly, Fig. 2(b) illustrates the entropy in the plane of temperature and perpendicular external magnetic field. Although the plot is quite similar to Fig. 2(a), there are some slight differences; for example, a strong change occurs at a slightly higher magnetic field $B_{\perp} \approx 5\text{T}$. It is also worth mentioning that in the absence of external magnetic field the system is twofold degenerate, so the entropy leads to $\mathcal{S} \to \ln(2)$.

C. Specific heat

Specific heat is of significant importance to the MCE because it fundamentally influences the amount of heat absorbed or released during the application or removal of a magnetic field. It quantifies the amount of heat required to change a compound temperature by a certain amount. Therefore, we
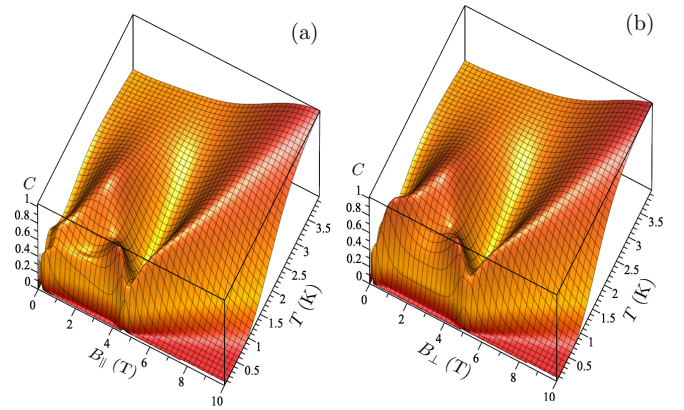

FIG. 3. (a) Specific heat C as a function of temperature and parallel external magnetic field. (b) Specific heat C as a function of temperature and perpendicular external magnetic field. For the Cu$_3$-As compound.

can use the following relation to obtain the specific heat:

$$C = \frac{\langle \mathbf{H}^2 \rangle - \langle \mathbf{H} \rangle^2}{T^2}, \tag{7}$$

where

$$\langle \mathbf{H}^2 \rangle = \frac{1}{Z} \sum_{i=1}^{8} \varepsilon_i^2 e^{-\varepsilon_i/T}. \tag{8}$$

It is worth mentioning that the specific heat can depend analytically on temperature, after eigenvalues are found numerically.

Figure 3(a) presents the specific heat as a function of temperature and the parallel external magnetic field $B_{\parallel}$. An anomalous behavior is noticeable at $B_{\parallel} \approx 4.5$ T, which manifests as an unusual peak in the low-temperature region. Additionally, two peculiar peaks appear at $B_{\parallel} \sim 2$ T, whereas other regions with a fixed magnetic field exhibit only one anomalous peak. Figure 3(b) illustrates an analogous plot, albeit with the perpendicular magnetic field $B_{\perp}$. The specific heat plots mainly resemble those in Fig. 3(a), with the exception of the absence of a minimum at $B_{\perp} \sim 2$ T. The low-temperature anomaly occurs at $B_{\parallel} \approx 5$ T. For a system with temperature around $T \sim 1$ K, the specific heat exhibits unusual behavior, absorbing or releasing heat more efficiently for a given temperature change. High specific heat is a beneficial property because it can enhance the overall efficiency and effectiveness of the triangular system. From the perspective of the MCE, this translates into more efficient magnetic cooling or heating.

D. Magnetization

We will now discuss magnetization, which plays a key role in the MCE. The strength of the MCE is directly related to the change in magnetization of the compound in response to variation in temperature and the applied magnetic field. In our case, the magnetization can be derived without taking numerical derivatives through the following relation:

$$\left\langle \left(\frac{\partial \mathbf{H}}{\partial B_k} \right) \right\rangle = \frac{1}{Z} \text{tr}\{ \mathbf{H}_{B_k} e^{-\mathbf{H}/T} \} = \frac{1}{Z} \text{tr}\{ \tilde{\mathbf{H}}_{B_k} e^{-\mathbf{E}/T} \}, \tag{9}$$
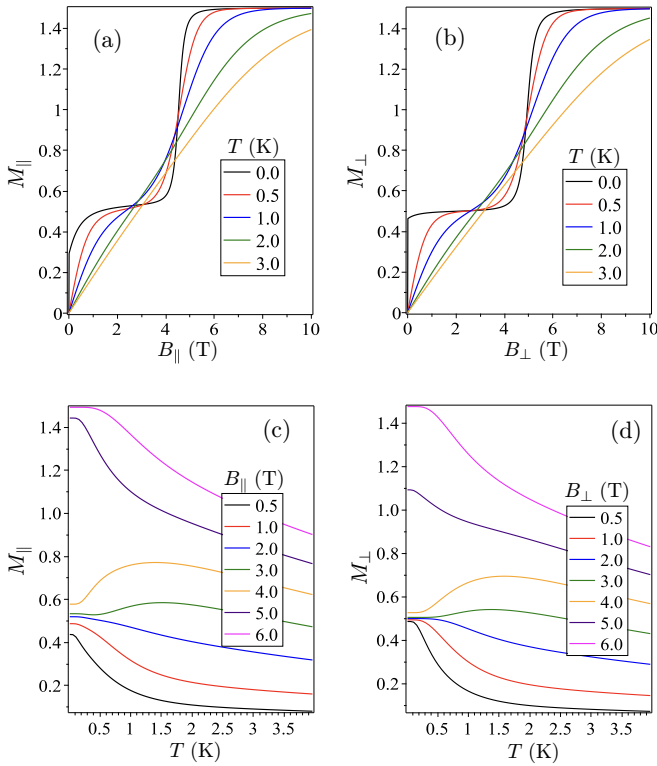
FIG. 5. (a) Magnetic susceptibility times temperature $T\chi_\parallel$ in the plane of temperature and parallel external magnetic field. (b) Magnetic susceptibility $T\chi_\perp$ in the plane of temperature and perpendicular external magnetic field.

magnetic field perpendicular to the triangular plane. The magnetization behavior closely resembles that in Fig. 4(c), but with a more noticeable convergence to the 1/3 quasiplateau in low-temperature regions. Here again, the main curvature change happens approximately at 1 K.

E. Magnetic susceptibility

Magnetic susceptibility is another relevant quantity for studying the MCE because it determines how easily a material can be magnetized or demagnetized. To obtain this quantity, we can follow a procedure similar to the previous one. Thus, the magnetic susceptibility can be written as

$$\chi_k = \frac{1}{\mathfrak{g}_k^2 T}\left\{\left\langle\left(\frac{\partial \mathbf{H}}{\partial B_k}\right)^2\right\rangle - \left\langle\left(\frac{\partial \mathbf{H}}{\partial B_k}\right)\right\rangle^2\right\}. \qquad (11)$$

Figure 5(a) illustrates the magnetic susceptibility times temperature $T\chi_\parallel$ for the Cu₃-As compound, plotted against temperature (in kelvins) and parallel external magnetic field (teslas). It is noteworthy that at $B_\parallel \approx 4.5$ T, $T\chi_\parallel$ maintains a constant value of around $T\chi_\parallel \approx 0.3$. This means that the magnetic susceptibility inversely depends on the temperature in the low-temperature region. A similar finite value is observed for the null magnetic field. This is due to the shift from regions dominated by two aligned spins and one oppositely aligned spin, leading to complete alignment with the external magnetic field. The Cu₃-X compound, with higher magnetic susceptibility, can be magnetized or demagnetized more readily, resulting in greater thermal energy transfer and a more significant temperature change, roughly at $T \lesssim 1$ K. Similarly, Fig. 5(b) depicts the product of magnetic susceptibility and temperature $T\chi_\perp$ in the plane of temperature and perpendicular external magnetic field. Although the behavior is quite similar to that in Fig. 5(a), there are slight differences, such as the pronounced change occurring at a slightly higher magnetic field, $B_\perp \approx 5$ T. Therefore, magnetic susceptibility affects the magnitude of the temperature change observed during the MCE and could play a crucial part in enhancing magnetic refrigeration systems.

FIG. 4. (a) Magnetization versus parallel magnetic field at various temperatures. (b) Magnetization versus perpendicular magnetic field at the same temperatures. (c) Temperature-dependent magnetization for different parallel magnetic fields for several parallel magnetic fields. (d) Analogously, temperature-dependent magnetization for a set of perpendicular magnetic fields. The study considers the Cu₃-As compound.

where $\tilde{\mathbf{H}}_{B_k} = \mathbf{U}(\frac{\partial \mathbf{H}}{\partial B_k})\mathbf{U}^{-1}$ and $k = \{\parallel, \perp\}$. This method is a typical procedure to avoid numerical derivatives, as the Hamiltonian can be derived in relation to B_k analytically. Therefore, the magnetization becomes

$$M_k = -\frac{1}{\mathfrak{g}_k}\left\langle\left(\frac{\partial \mathbf{H}}{\partial B_k}\right)\right\rangle, \qquad (10)$$

where $\mathfrak{g}_k$ is a constant normalization chosen for convenience, defined as follows: $\mathfrak{g}_k = \frac{1}{3}\sum_{i=1}^{3} g_i^k$. The values of $\mathfrak{g}_\parallel$ are 2.25 for both compounds, while the values of $\mathfrak{g}_\perp$ are 2.06 and 2.07 for As and Sb, respectively.

Figure 4(a) presents the magnetization as a function of the parallel magnetic field $B_\parallel$ at various temperature values, including zero temperature. Note that a 1/3 quasiplateau feature appears, fading as temperature increases to around 1 K. Similarly, Fig. 4(b) reports magnetization as a function of a perpendicular external magnetic field. Here, the 1/3 quasiplateau becomes more noticeable, with effects largely mirroring those in Fig. 4(a). Conversely, Fig. 4(c) displays magnetization as a function of temperature, considering multiple external magnetic fields parallel to the triangular plane. In this panel, the quasiplateau region converges to $M \sim 0.5$, with a saturated region at $M \to 1.5$. A significant curvature change occurs at around 1 K. Last, Fig. 4(d) illustrates the magnetization as a function of temperature for an external
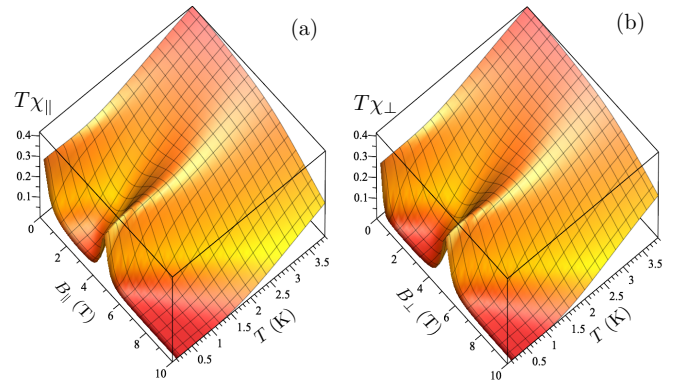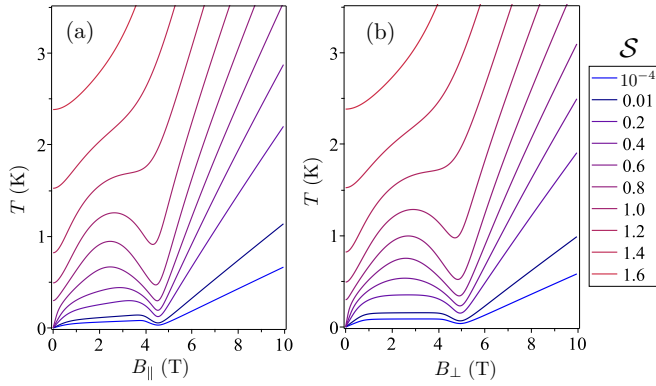
FIG. 6. (a) Plot of isentropic $\mathcal{S}$ (in units of k_B) curve temperature T (K) versus a parallel magnetic field $B_\parallel$ (T). (b) Plot of isentropic curve temperature T (K) as a function of magnetic field $B_\perp$ (T). Both plots are for the Cu$_3$-As compound.

IV. MAGNETOCALORIC EFFECT

The magnetocaloric effect refers to the thermal response of a material to the change in an external magnetic field. It holds potential for practical applications such as energy-efficient cooling technologies. Accordingly, we will discuss aspects such as the isentropic curve and Grüneisen parameter.

A. Isentropic curve

In magnetic systems, isentropic curves or adiabatic temperature curves provide a useful tool to visualize and understand the MCE. In the context of the MCE, an isentropic curve represents a process that occurs at constant entropy in a magnetic-field-temperature phase diagram.

In Fig. 6(a), the isentropic curve for {Cu$_3$-As} is illustrated for a parallel magnetic field. Between null magnetic field and $B_\parallel \approx 4.5$ T, the system exhibits the first step of magnetization, with two spins aligned parallel to the magnetic field while the third one is aligned antiparallel. For $B_\parallel \gtrsim 4.5$ T, all spins become aligned with the magnetic field. The isentropic curve shows high sensitivity at relatively low entropy, and as temperature increases, the crossover region between these two states manifests as a minimum. This minimum gradually disappears around $T \sim 1$ K. Notably, strong slopes of the isentropic curves occur around the minimum, indicating a large MCE in this region. Similarly, in Fig. 6(b), the isentropic curve for {Cu$_3$-As} is depicted for a perpendicular magnetic field. The behavior of the isentropic curve is largely analogous to the previous case, with the only difference being that the minimum occurs at approximately $B_\perp \approx 5$ T. These curves provide insight into the temperature changes in a system in response to the application or removal of an external magnetic field. Additionally, the shape of the isentropic curve can provide valuable information about possible zero-temperature magnetic phase transitions in the {Cu$_3$-As} compound.

B. Grüneisen parameters

The Grüneisen parameter plays an essential role in understanding the MCE, which refers to the change in temperature of a material resulting from variations in an applied
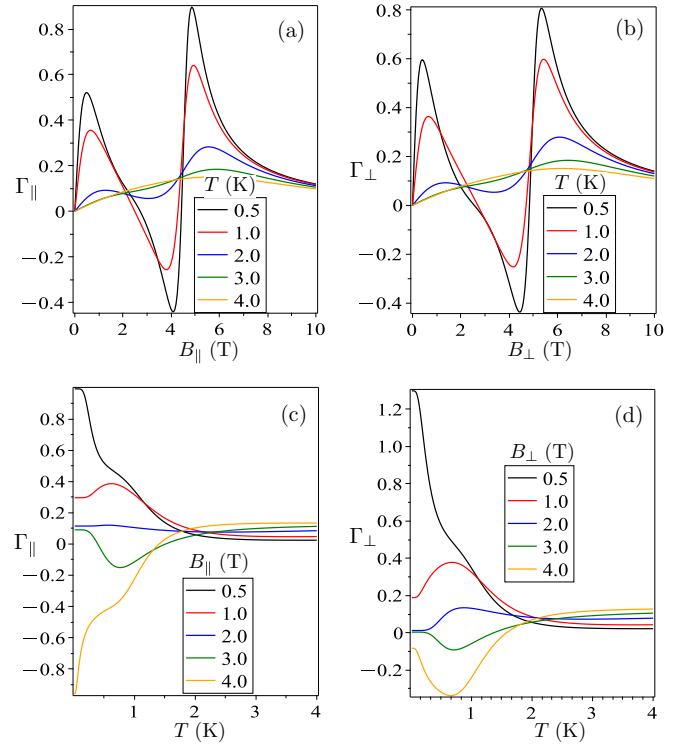

FIG. 7. (a) Grüneisen parameter $\Gamma_\parallel$ as a function of parallel magnetic field $B_\parallel$ for a range of temperatures. (b) Grüneisen parameter $\Gamma_\perp$ as a function of perpendicular magnetic field. (c) $\Gamma_\parallel$ as a function of temperature for a set of parallel magnetic fields. (d) $\Gamma_\perp$ as a function of temperature for a number of perpendicular magnetic fields. The magnetic field is in teslas, while temperature is measured in kelvins. For the Cu$_3$-As compound.

magnetic field. This effect has significant applications in magnetic cooling technologies. The Grüneisen parameter quantifies the relationship between the change in temperature of the compound and the magnetic field under constant entropy conditions. Specifically, the Grüneisen parameter Γ is defined as the ratio of the temperature derivative of the magnetization per mole to the molar specific heat,

$$\Gamma_k = -\frac{1}{C}\left(\frac{\partial M}{\partial T}\right)_{B_k} = -\frac{\left(\frac{\partial \mathcal{S}}{\partial B_k}\right)_T}{T\left(\frac{\partial \mathcal{S}}{\partial T}\right)_{B_k}} = \frac{1}{T}\left(\frac{\partial T}{\partial B_k}\right)_{\mathcal{S}}. \quad (12)$$

To avoid numerical derivatives, an equivalent expression for the Grüneisen parameter can be derived:

$$\Gamma_k = \frac{1}{\mathfrak{g}_k}\frac{\langle \mathbf{H}_{B_k}\mathbf{H}\rangle - \langle \mathbf{H}_{B_k}\rangle\langle \mathbf{H}\rangle}{\langle \mathbf{H}^2\rangle - \langle \mathbf{H}\rangle^2}. \quad (13)$$

Other research has explored these phenomena by analyzing the adiabatic temperature change, which demonstrates a strong correlation with the magnetic entropy change [37].

In Fig. 7(a), the Grüneisen parameter is illustrated as a function of the parallel magnetic field $B_\parallel$ for various fixed temperatures. The Grüneisen parameter shows significant changes in response to an applied magnetic field, with the most notable variations occurring at $B_\parallel \sim 1$ T for temperatures around $T \sim 1$ K. As the temperature increases, the magnitude of these changes decreases. Another region where the Grüneisen parameter becomes relevant is around

$B_\parallel \approx 4.5\,\text{T}$, exhibiting a strong variation. However, as the temperature increases, the magnitude of the Grüneisen parameter at this field strength decreases, eventually diminishing. Figure 7(b) presents an equivalent quantity obtained by applying a perpendicular magnetic field $B_\perp$, yielding results equivalent to the previous case. Additionally, in Fig. 7(c), we depict the variation of Γ as a function of temperature for different external parallel magnetic fields. A significant change in the Grüneisen parameter $\Gamma_\parallel$ is observed for temperatures below $T \sim 2$ K. When the magnetic field is lower than $B_\parallel \sim 2$ T, $\Gamma_\parallel$ is positive, whereas for $B_\parallel \gtrsim 2$ T, this parameter becomes negative. Moreover, for temperatures $T \gtrsim 2$ K, the Grüneisen parameter decreases significantly. Figure 7(d) is similar to Fig. 7(c), but for a perpendicular magnetic field. Some differences arise, such as a stronger $\Gamma_\perp$ compared to the parallel case for low magnetic fields ($B_\perp \sim 0.5$ T) and the low-temperature region. Conversely, for large magnetic fields ($B_\perp \sim 4.0$ T), the Grüneisen parameter $\Gamma_\perp$ is weaker than in the parallel case. In conclusion, the study of Cu₃-As reveals a significant Grüneisen parameter at around $B \sim 5$ T, indicating a prominent MCE. This finding holds crucial implications for the selection and design of magnetic refrigeration systems.

Last, but not least, the MCE can also be analyzed through the variation in entropy, $\Delta\mathcal{S} = \mathcal{S}(0, T) - \mathcal{S}(B, T)$, associated with the magnetic phase. This variation occurs due to the alignment or realignment of spins, resulting in changes in the disorder and order of the Cu₃-X compound and leading to a temperature change. Therefore, $\Delta\mathcal{S}$ is an important quantity for exploring the magnetocaloric performance.

In Fig. 8(a), we illustrate $\Delta\mathcal{S}$ as a function of the parallel external magnetic field $B_\parallel$ for several fixed temperatures. We observe that at a temperature of $T \sim 0.1$ K, the entropy remains almost constant [$\Delta\mathcal{S} \sim \ln(2) \approx 0.7$]. This is due to the system being roughly doubly degenerate at null magnetic field, and the degeneracy is broken by the presence of a magnetic field. There is a slight depression at $T \approx 4.5$ K, indicating a change in the dominant phases at this magnetic field. This behavior changes significantly as the temperature increases. For $B_\parallel \lesssim 4.5$ T, $\Delta\mathcal{S}$ decreases significantly, while for $B_\parallel \gtrsim 4.5$ T, it becomes larger. Figure 8(b) shows analogous behavior, but for the perpendicular external magnetic field $B_\perp$. The only difference is that the depression occurs at $B_\perp \lesssim 5.0$ T. Furthermore, in Fig. 8(c), we present $\Delta\mathcal{S}$ as a function of temperature for several fixed parallel magnetic fields $B_\parallel$. For magnetic fields below $B_\parallel \lesssim 4.5$ T, $\Delta\mathcal{S}$ decreases monotonically. However, for stronger magnetic fields $B_\parallel \gtrsim 4.5$ T, a maximum appears, indicating a peak in $\Delta\mathcal{S}$. Similarly, Fig. 8(d) depicts $\Delta\mathcal{S}$ as a function of temperature, assuming a fixed perpendicular magnetic field. The behavior is very similar to Fig. 8(c), although $\Delta\mathcal{S}$ does not decrease monotonically. Additionally, for strong magnetic fields, it also exhibits a maximum, as observed in Fig. 8(c).

V. CONCLUSIONS

In this paper, we conducted a theoretical exploration of the Cu₃-X antiferromagnetic spin system (where X=As, Sb), which is identified by its isosceles or slightly distorted equilateral triangular configurations, as detailed in Refs. [21,23,24]. This system can be accurately depicted using the Heisenberg
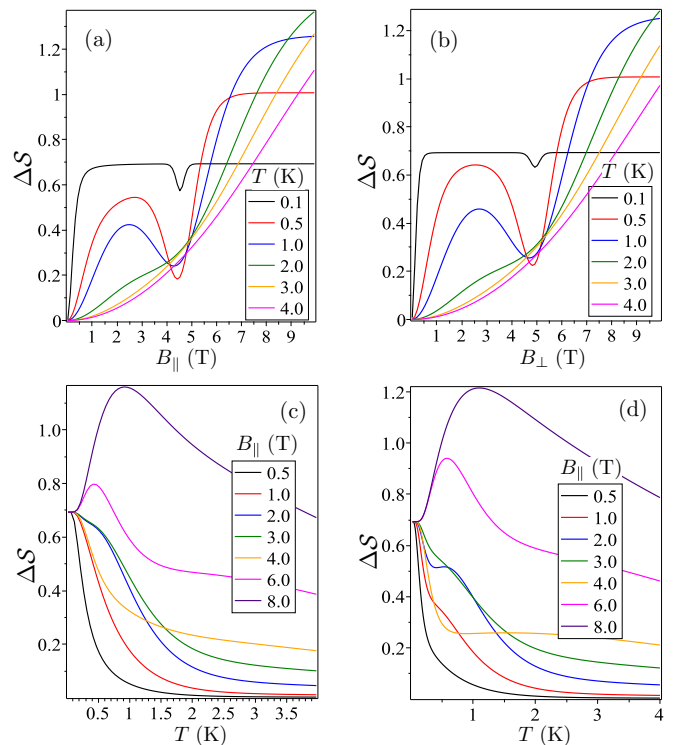

FIG. 8. (a) Entropy variation $\Delta\mathcal{S}$ as a function of parallel magnetic field $B_\parallel$ for a set of fixed temperatures. (b) Entropy variation $\Delta\mathcal{S}$ as a function of perpendicular magnetic field. (c) $\Delta\mathcal{S}$ as a function of temperature for a variety of parallel magnetic fields. (d) $\Delta\mathcal{S}$ as a function of temperature for different perpendicular magnetic fields.

model on a triangular structure, incorporating factors like the exchange interaction, Dzyaloshinskii-Moriya interaction, g factors, and external magnetic fields.

Recently, Cu₃-X has garnered significant attention due to its fundamental properties [21,23,24]. Furthermore, the scientific community has shown a growing interest in the exploration of several magnetic compounds [25–31] due to their diverse possibilities in areas such as spintronics, nanotechnology, and biomedicine.

Our investigation used a numerical approach to analyze both zero-temperature and finite-temperature behaviors of the Cu₃-type spin system. At zero temperature, the system exhibits twofold degenerate energy in the absence of a magnetic field and a 1/3 quasiplateau magnetization when the magnetic field is varied. At finite temperatures, our focus was primarily on analyzing magnetic properties such as magnetization, magnetic susceptibility, entropy, and specific heat.

In addition, we examined the MCE in relation to an externally applied magnetic field, oriented both parallel and perpendicular to the plane of the triangular structure. Cu₃-X displays remarkably consistent behavior for both orientations of the magnetic field. We also extended our study to include an evaluation of the isentropic curve, the Grüneisen parameter, and the variation in entropy during the application or removal of the magnetic field. Therefore, in the low-temperature region below $T \sim 1$ K and for approximately 4.5 and 5 T for parallel and perpendicular magnetic fields, respectively, our results confirm that the MCE is more prominent in this region.

This study could contribute to the research and development of nanocompounds with triangular structures, potentially improving the performance of the magnetocaloric effect. Such advancements may be especially intriguing for applications in the cryogenic temperature range that utilize moderate magnetic fields.

[1] O. Tegus, E. Brück, K. H. J. Buschow, and F. R. de Boer, Transition-metal-based magnetic refrigerants for room-temperature applications, Nature (London) **415**, 150 (2002).

[2] T. Gruner, D. Kim, M. Brando, A. V. Dukhnenko, N. Y. Shitsevalova, V. B. Filipov, and D. Jang, Reversible and irreversible magnetocaloric effect: The cases of rare-earth intermetallics $YbPt_2Sn$ and $Ce_{0.5}La_{0.5}B_6$, J. Magn. Magn. Mater. **489**, 165389 (2019).

[3] K. A. Gschneidner, Jr., V. K. Pecharsky, and A. O. Tsokol, Recent developments in magnetocaloric materials, Rep. Prog. Phys. **68**, 1479 (2005).

[4] J. Liu, T. Gottschall, K. P. Skokov, J. D. Moore, and O. Gutfleisch, Giant magnetocaloric effect driven by structural transitions, Nat. Mater. **11**, 620 (2012).

[5] J. Darby, J. Hatton, B. V. Rollin, E. F. W. Seymour, and H. B. Silsbee, Experiments on the production of very low temperatures by two-stage demagnetization, Proc. Phys. Soc. London, Sect. A **64**, 861 (1951).

[6] G. V. Brown, Magnetic heat pumping near room temperature, J. Appl. Phys. **47**, 3673 (1976).

[7] V. K. Pecharsky and K. A. Gschneidner, Jr., Giant magnetocaloric effect in $Gd_5(Si_2Ge_2)$, Phys. Rev. Lett. **78**, 4494 (1997).

[8] C. Zimm, A. Jastrab, A. Sternberg, V. K. Pecharsky, K. A. Gschneidner, Jr., M. Osborne, and I. Anderson, Description and performance of a near-room temperature magnetic refrigerator, Adv. Cryog. Eng. **43**, 1759 (1998).

[9] V. K. Pecharsky, K. A. Gschneidner, Jr., A. O. Pecharsky, and A. M. Tishin, Thermodynamics of the magnetocaloric effect, Phys. Rev. B **64**, 144406 (2001).

[10] D. N. Ba, L. Becerra, N. Casaretto, J. E. Duvauchelle, M. Marangolo, S. Ahmim, M. Almanza, and M. LoBue, Magnetocaloric gadolinium thick films for energy harvesting applications, AIP Adv. **10**, 035110 (2020).

[11] D. Nguyen Ba, Y. Zheng, L. Becerra, M. Marangolo, M. Almanza, and M. LoBue, Magnetocaloric effect in flexible, free-standing gadolinium thick films for energy conversion applications, Phys. Rev. Appl. **15**, 064045 (2021).

[12] F. Zhang, C. Taake, B. Huang, X. You, H. Ojiyed, Q. Shen, I. Dugulan, L. Caron, N. van Dijk, and E. Brücka, Magnetocaloric effect in the $(Mn, Fe)_2(P, Si)$ system: From bulk to nano, Acta Mater. **224**, 117532 (2022).

[13] K. Klinar, M. M. Rojo, Z. Kutnjak, and A. Kitanovski, Toward a solid-state thermal diode for room-temperature magnetocaloric energy conversion, J. Appl. Phys. **127**, 234101 (2020).

[14] V. Chaudhary, Z. Wang, A. Ray, I. Sridhar, and R. V. Ramanujan, Self pumping magnetic cooling, J. Phys. D **50**, 03LT03 (2017).

[15] M. S. Pattanaik, S. K. Cheekati, V. B. Varma, and R. V. Ramanujan, A novel magnetic cooling device for long

distance heat transfer, Appl. Therm. Eng. **201**, 117777 (2022).

[16] U. Sen, S. Chatterjee, S. Sen, M. K. Tiwari, A. Mukhopadhyay, and R. Ganguly, A novel magnetic cooling device for long distance heat transfer, J. Magn. Magn. Mater. **421**, 165 (2017).

[17] M. Qian, X. Zhang, L. Wei, P. Martin, J. Sun, L. Geng, T. B. Scott, and H.-X. Peng, Tunable magnetocaloric effect in Ni-Mn-Ga microwires, Sci. Rep. **8**, 16574 (2018).

[18] X. L. Liu, Y. F. Zhang, Y. Y. Wang, W. J. Zhu, G. L. Li, X. W. Ma, Y. H. Zhang, S. Z. Chen, S. Tiwari, K. J. Shi, S. W. Zhang, H. M. Fan, Y. X. Zhao, and X. J. Liang, Comprehensive understanding of magnetic hyperthermia for improving antitumor therapeutic efficacy, Theranostics **10**, 3793 (2020).

[19] J. B. Li, Y. Qu, J. Ren, W. Z. Yuan, and D. L. Shi, Magnetocaloric effect in magnetothermally-responsive nanocarriers for hyperthermia-triggered drug release, Nanotechnology **23**, 505706 (2012).

[20] T. Yamase, E. Ishikawa, K. Fukaya, H. Nojiri, T. Taniguchi, and T. Atake, Spin-frustrated $(VO)_3^{6+}$-triangle-sandwiching octadecatungstates as a new class of molecular magnets, Inorg. Chem. **43**, 8150 (2004).

[21] K.-Y. Choi, Y. H. Matsuda, and H. Nojiri, Observation of a half step magnetization in the {Cu$_3$} -type triangular spin ring, Phys. Rev. Lett. **96**, 107202 (2006).

[22] M. Trif, F. Troiani, D. Stepanenko, and D. Loss, Spin-electric coupling in molecular magnets, Phys. Rev. Lett. **101**, 217201 (2008).

[23] K.-Y. Choi, N. S. Dalal, A. P. Reyes, P. L. Kuhns, Y. H. Matsuda, H. Hojiri, S. S. Mal, and U. Kortz, Pulsed-field magnetization, electron spin resonance, and nuclear spin-lattice relaxation in the {Cu$_3$} spin triangle, Phys. Rev. B **77**, 024406 (2008).

[24] K.-Y. Choi, Z. Wang, H. Nojiri, J. van Tol, P. Kumar, P. Lemmens, B. S. Bassil, U. Kortz, and N. S. Dalal, Coherent manipulation of electron spins in the {Cu$_3$} spin triangle complex impregnated in nanoporous silicon, Phys. Rev. Lett. **108**, 067206 (2012).

[25] M.-A. Bouammali, N. Suaud, N. Guihéry, and R. Maurice, Antisymmetric exchange in a real copper triangular complex, Inorg. Chem. **61**, 12138 (2022).

[26] E. T. Spielberg, A. Gilb, D. Plaul, D. Geibig, D. Hornig, D. Schuch, A. Buchholz, A. Ardavan, and W. Plass, A spin-frustrated trinuclear copper complex based on triaminoguanidine with an energetically well-separated degenerate ground state, Inorg. Chem. **54**, 3432 (2015).

[27] M. I. Belinsky, Spin chirality of Cu$_3$ and V$_3$ nanomagnets. 2. Frustration, temperature, and distortion dependence of spin chiralities and magnetization in the rotating and tilted magnetic fields, Inorg. Chem. **55**, 4091 (2016).

[28] J. Robert, N. Parizel, P. Turek, and A. K. Boudalis, Relevance of Dzyaloshinskii–Moriya spectral broadenings in

promoting spin decoherence: A comparative pulsed-EPR study of two structurally related iron(iii) and chromium(iii) spin-triangle molecular qubits, Phys. Chem. Chem. Phys. **21**, 19575 (2019).

[29] A. K. Boudalis, Half-integer spin triangles: Old dogs, new tricks, Chem. A Eur. J. **27**, 7022 (2021).

[30] A. C. Stowe, S. Nellutla, N. S. Dalal, and U. Kortz, Magnetic properties of lone-pair-containing, sandwich-type polyoxoanions: A detailed study of the heteroatomic effect, Eur. J. Inorg. Chem. **2004**, 3792 (2004).

[31] U. Kortz, S. Nellutla, A. C. Stowe, N. S. Dalal, J. van Tol, and B. S. Bassil, Structure and magnetism of the tetra-copper(II)-substituted heteropolyanion $[Cu_4K_2(H_2O)_8(\alpha\text{-}AsW_9O_{33})_2]^{8-}$, Inorg. Chem. **43**, 144 (2004).

[32] P. Kowalewska and K. Szałowski, Magnetocaloric properties of V6 molecular magnet, J. Magn. Magn. Mater. **496**, 165933 (2020).

[33] K. Karľová, J. Strečka, and J. Richter, Enhanced magnetocaloric effect in the proximity of magnetization steps and jumps of spin-1/2 XXZ Heisenberg regular polyhedra, J. Phys.: Condens. Matter **29**, 125802 (2017).

[34] J. Torrico and J. A. Plascak, Ground state and thermodynamic properties of spin-1/2 isosceles Heisenberg triangles for V_6-like magnetic molecules, Phys. Rev. E **102**, 062116 (2020).

[35] J. Torrico and J. A. Plascak, Study of the ground state and thermodynamic properties of Cu_5-NIPA-like molecular nanomagnets, J. Magn. Magn. Mater. **552**, 169151 (2022).

[36] P. J. von Ranke and W. S. Torres, Theoretical investigation of crystalline electric field influence on the magnetocaloric effect in the cubic praseodymium system $PrNi_2$, Phys. Rev. B **105**, 085153 (2022).

[37] L. Zhu, M. Garst, A. Rosch, and Q. Si, Universally diverging Grüneisen parameter and the magnetocaloric effect close to quantum critical points, Phys. Rev. Lett. **91**, 066404 (2003).